

Article

Vibro-Acoustic Performance of a Sandwich Plate with Periodically Inserted Resonators

Zhiwei Guo ¹, Jie Pan ² and Meiping Sheng ^{1,*}¹ School of Marine Science and Technology, Northwestern Polytechnical University, Xi'an 710072, China² School of Mechanical and Chemical Engineering, The University of Western Australia, Perth 6009, Australia

* Correspondence: smp@nwpu.edu.cn; Tel.: +86-029-8849-5861

Received: 21 July 2019; Accepted: 23 August 2019; Published: 4 September 2019



Abstract: The vibro-acoustic performance of a sandwich plate with periodic locally resonant (LR) units is examined in this paper, with specific focus on the effect of periodic resonators on the average radiation efficiency and the acoustic radiation to the far field. In order to assess the radiation performance, the band-gap properties of an infinite periodic structure and the vibrational response of a finite periodic structure are first studied with closed-form solutions. Subsequently, the acoustic radiation efficiency of the LR sandwich plate is obtained using the concepts of modal radiation. It is shown that the acoustic radiation power can be reduced significantly, not only in the band-gap but also at frequencies close below the band-gap, due to either the decrease in radiation efficiency or the decrease in the vibration response. Thus, the periodic resonators provide a broader attenuation band for the purposes of noise reduction than for vibration reduction. However, for frequencies close above the band-gap, the acoustic performance became worse, owing to the increase in acoustic radiation efficiency. Fortunately, the increased sound radiation above the band-gap can be reduced by adding a small damping to the resonator, which further broadens the attenuation frequency band. The reason for the variation of acoustic radiation efficiency is also studied and can be physically explained by the effective mass of an LR unit, where increased mass corresponds to decreased radiation efficiency and decreased mass corresponds to increased radiation efficiency. Thus, the effective mass can be a useful parameter for designers to estimate which frequency component will be acoustically reduced or acoustically enhanced in a practical design.

Keywords: periodic sandwich plate; periodically inserted resonators; radiation efficiency; vibro-acoustic reduction; local-resonance band-gap

1. Introduction

Sandwich structures have been researched for centuries and are one of the most used structures in industry, including but not limited to airplane [1], automobile [2], underwater vehicle [3], and architecture [4]. In general, a sandwich structure usually consists of two high-strength surfaces and one low-strength and also low-density core. Configured by this, sandwich structures can provide an increased stiffness-to-mass ratio compared with both stiffened plates and homogeneous plates when they have the same mass, owing to the increased rotational inertia and bending rigidity for sandwich structures. The stiffness-to-mass ratio plays a very important role in engineering design when the goal of design optimization is reducing weight.

As sandwich structures have great potential in application, a quite number of researches can be obtained from the public literatures, with various focus on building theoretical models [5–8], researching dynamic properties [9–11], configuring structures with various types of cores [12–18], and also realizing the engineering applications [1–4]. In practice, sandwich structures have various configurations for various specific focus, with the main difference lying on the cores. In the aircrafts,

honeycomb cores [13,18] are usually used in order to obtain both enough strength and also light weight. When the core is designed with heat-insulating material [19,20], the sandwich structures can not only be used in the building walls to maintain temperature of the inner space but also can be applied in a missile to protect the internal precision equipment. Another example is that a sandwich plate with a porous core [15] can be used for noise-isolation purpose.

As seen in the above, sandwich structures have many attractive characteristics in the engineering. However, some light-weight sandwich structures may induce acoustic problem, as these light-weight structures vibrate and radiate annoying noise easily. Efforts have been made to improve the poor acoustical performance by using a viscoelastic material core [14], by optimal sandwich design [21–23], by applying a magnetorheological core or electrorheological core [12,16], and also by introducing an active surface panel [24,25].

In recent decades, numerical researches about periodic structures including both phononic crystals [26–28] and metamaterials [29–31] have been conducted, as they can effectively attenuate vibration and then reduce noise radiation. Owing to spatial periodicity of periodic structures, waves of some specific frequencies cannot propagate without attenuation while other waves can propagate successfully. In this wave-filtering phenomenon, the frequency band where waves cannot propagate forms a band-gap. In the band-gap, no wave can propagate and thus the vibration can be significantly attenuated. Therefore, periodic structures have steadily come to be considered as a new method to improve vibro-acoustic performance.

Researches have shown that Bragg scattering mechanism [32] and locally resonant mechanism [27] are two main mechanisms for the formation of a band-gap. For a locally resonant (LR) periodic structure, the resonance of the resonators is the main cause of the band-gap, and it has been found that the working wavelength of an LR periodic structure can be far greater than the lattice constant (the dimensions of a unit in the periodic structure). Therefore, the LR periodic structure has the ability to reduce lower frequency than a Bragg-scattering structure. Liu et al. [27] first proposed the concept of an LR phononic crystal and verified this type of band-gap with a carefully designed specimen, where lead balls are coated with silicon rubber and they are embedded in an epoxy-matrix plate. By doing this, they obtained an LR band-gap far lower than traditional Bragg band-gap frequencies. Attracted by its low-frequency band-gap performance, the LR periodic structure has been widely studied by researchers in recent years and various configurations of plate-type structures have been proposed. As summarized by Wu et al. [33], several types of configurations have been proposed to meet the requirements of practical applications, including periodic resonators inserted in the periodic openings of a plate [34–38], mounted at the surface of a homogeneous plate [39–41], and also embedded in a close plate with great thickness [42].

Most studies in the available literature about LR structures are related to a single-layer plate, while very few are related to composite laminate structures, owing to their complexity. As the core of a sandwich panel typically has great thickness, it is possible to insert resonators into the core. With the urgent need for vibration control in sandwich panels, Chen and Sun [43] were the first to introduce spring–mass resonators to a sandwich beam in order to study its unusual dynamic behavior with two proposed theoretical continuum models. The initial work was followed and extended by their research group [44–49] with a specific focus on new theories, practical experiments, the combined effects of periodic resonators and periodic cores, and also the improvement from a single resonator to multiple resonators. These studies were limited to vibrational dynamic behavior and one-dimensional sandwich structures, where acoustic radiation was not considered and cross-stream mode induced by multi-dimension was also not involved. However, in practical applications, most sandwich panels are designed in two dimensions, and sometimes the vibration-induced sound radiation is the major concern except vibration response.

Thus, in this paper, the LR sandwich beam is extended to a sandwich plate to meet the practical needs of applications. In addition, the main purpose of this paper is to study the acoustic radiation behavior. For an LR periodic structure, most studies have focused on the effects of the band-gap on

vibrational dynamic behavior. However, the effects of the band-gap on sound radiation cannot be represented by or inferred from the effects on vibration, as the sound radiation is not only dependent on vibration response, but also dependent on radiation efficiency. Thus, the study of vibro-acoustic performance of a sandwich plate with periodically inserted resonators has practical meaning.

In this paper, the vibro-acoustic performance of an LR sandwich plate is examined, with specific focus on sound radiation performance caused by periodic resonators. A closed-form solution for an LR sandwich plate is theoretically derived. The dispersion curve and the band-gap are obtained by using governing equations for a sandwich plate and Bloch boundary conditions. Then the vibrational response of a finite LR sandwich plate is given to examine the effects of periodic resonators on vibrational performance. In the following, the vibration-induced sound radiation power and corresponding radiation efficiency are studied to examine the acoustic performance of an LR sandwich plate. The variation of acoustic performance is physically explained by the effective mass, and the effect of damping of the resonator to provide more beneficial acoustic performance is also discussed. The findings in this paper provide guidance for band-gap design in an LR sandwich plate when the purpose is not only on the reduction of vibration but also on the reduction of sound radiation.

2. Formulations

2.1. Structure Model and Governing Equations

A unit element of a periodic LR sandwich plate is shown in Figure 1, where a resonator consisting of a mass block and two linear springs is mounted in a cylindrical hollow in the core layer of a symmetric sandwich plate. In this coupled system, the mass block is connected to the top and bottom surface layers with two identical linear springs. Thus, in the LR band-gap, the vibration energy of the surface panels can be transmitted to the inner mass and most of the system energy will be stored in the periodic resonators. The change in vibration distribution and the change in radiation efficiency induced by coupling between the sandwich panel and its inserted periodic resonators will lead to a change in the corresponding acoustic radiation.

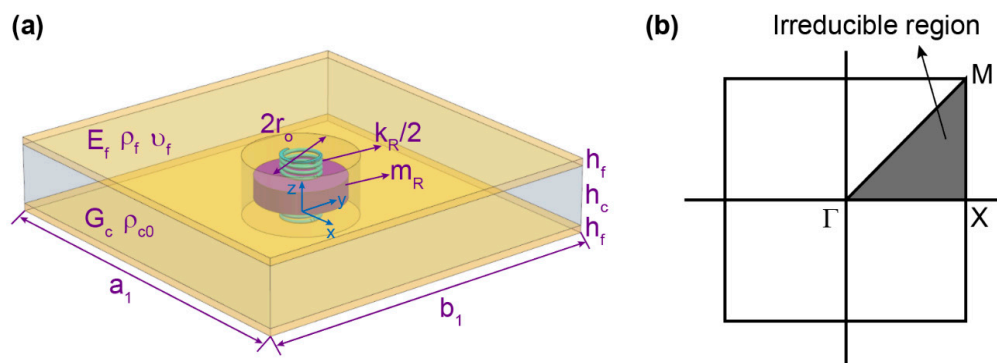


Figure 1. (a) Configuration of a unit element and (b) the first Brillouin zone.

The unit element of the LR sandwich plate has the dimensions of length a_1 , width b_1 , surface-layer thickness h_f , and core thickness h_c . The material parameters of the surface layer are the Young’s modulus E_f , density ρ_f , and Poisson’s ratio ν_f , while the material parameters of the core layer are the shear modulus G_c and density ρ_{c0} . Each linear spring has identical stiffness $k_R/2$ and the mass of the resonator is denoted as m_R . In addition, the radius of the inner cylindrical hollow is r_o .

In the following theoretical model, an inhomogeneous sandwich plate with periodic cylindrical hollows is modeled as a homogeneous sandwich plate with an equivalent density of the core expressed as $\rho_c = \rho_{c0}(1 - \pi r_o^2/a_1 b_1)$ and the resonator is assumed to be attached under the homogeneous sandwich plate with a mass m_R and a spring stiffness k_R . In addition, the shear moduli of the surface layers are dramatically larger than that of the inner core. Thus, the surface layers are assumed to

suffer longitudinal strain but no transverse shear strain, while the core layer suffers shear strain but no normal strain. In addition, the surface layers and the core layer are configured in perfect continuity and at the interfaces between each layer no slip occurs. The transverse displacements in each layer keep identical at the same in-plane position. Harmonic motion with a time-dependence term $e^{j\omega t}$ is considered throughout the paper.

Following the above assumptions, the strain energy of the surface layer and the core layer can be expressed respectively as

$$U_f = \frac{1}{2}B \int \int \left[u_x^2 + 2v_f u_x v_y + v_y^2 + v_a (u_y + v_x)^2 \right] dx dy + \frac{1}{2}D \int \int \left[w_{xx}^2 + 2v_f w_{xx} w_{yy} + w_{yy}^2 + 2(1 - v_f) w_{xy}^2 \right] dx dy \quad (1)$$

and

$$U_c = \frac{1}{2}G_h \int \int (\gamma_x^2 + \gamma_y^2) \quad (2)$$

where u , v , and w are the x -wise, y -wise, and z -wise surface displacements, respectively. The terms γ_x and γ_y are the shear strains of the sandwich core and are expressed, respectively, as $\gamma_x = (2u - dw_x)/h_c$ and $\gamma_y = (2v - dw_y)/h_c$, where $d = h_c + h_f$. In addition, $B = E_f h_f / (1 - \nu_f^2)$, $D = E_f h_f^3 / 12 (1 - \nu_f^2)$, $v_a = (1 - \nu_f) / 2$, and $G_h = G_c / h_c$.

The kinetic energies of the surface and core layers are expressed, respectively, as

$$T_f = \frac{1}{2} \int \int \left[m_f (\dot{u}^2 + \dot{v}^2 + \dot{w}^2) + I_f (\dot{w}_x^2 + \dot{w}_y^2) \right] dx dy \quad (3)$$

and

$$T_c = \frac{1}{2} \int \int \left\{ m_c (\dot{u}_c^2 + \dot{v}_c^2 + \dot{w}^2) + I_c \left[(\dot{\theta}_c)^2 + (\dot{\varphi}_c)^2 \right] \right\} dx dy \quad (4)$$

where $m_f = \rho_f h_f$, $m_c = \rho_c h_c$, $I_f = \rho_f h_f^3 / 12$, $I_c = \rho_c h_c^3 / 12$, $\theta_c = (2u - h_f w_x) / h_c$, and $\varphi_c = (2v - h_f w_y) / h_c$. Thus, the total strain energy and the total kinetic energy can be expressed as $U = 2U_f + U_c$ and $T = 2T_f + T_c$, respectively. By using Hamilton's principle, $\delta \int_0^{t_1} (T - U) dt = 0$, the governing equations of a sandwich plate can be obtained as

$$\mathbf{L}\mathbf{u} = \mathbf{f} \quad (5)$$

where $\mathbf{u} = [u \ v \ w]^T$ is a displacement vector and \mathbf{L} is a 3×3 operator matrix, which is defined in Equations (A1)–(A9) in Appendix A. The term $\mathbf{f} = [0 \ 0 \ f_e + f_{Rd}]^T$ is a force vector, where f_e is an external transverse force and $f_{Rd} = f_R \delta(x - x_R) \delta(y - y_R)$ is the force from the resonator, in which f_R is the force amplitude applied at the resonator position (x_R, y_R) . Force analysis on a resonator coupling with a sandwich unit shows that

$$\begin{cases} -f_R = m_R \ddot{w}_{R0} \\ f_R = -k_R [w(x_R, y_R) - w_{R0}] \end{cases} \quad (6)$$

where $w(x_R, y_R)$ and w_{R0} are the transverse displacement of the sandwich plate at position (x_R, y_R) and the displacement of the mass block of the resonator, respectively.

2.2. Band-Gap of, and Sound Radiation from, an Infinite Periodic Structure

2.2.1. Band-Gap

The plane-wave-expansion (PWE) method is used to study the band-gap properties of the LR sandwich plate. For an infinite sandwich plate, there are infinite resonators located periodically in the

x and y directions. Thus, the total force generated by the periodic resonators on the sandwich plate can be expressed as

$$f_{Rd} = \sum_{s=-\infty}^{\infty} \sum_{t=-\infty}^{\infty} f_{Rst} \delta(x - x_s) \delta(y - y_t), \tag{7}$$

where $(x_s = sa_1, y_t = ta_2)$ is the position of the st^{th} resonator and f_{Rst} is the force applied on the sandwich plate by the st^{th} resonator. According to the PWE method, the displacements of the LR sandwich plate can be written as

$$\begin{cases} u(x, y) = \sum_{m=-\infty}^{\infty} \sum_{n=-\infty}^{\infty} U_{mn} e^{-j(G_m + \alpha)x} e^{-j(G_n + \beta)y} \\ v(x, y) = \sum_{m=-\infty}^{\infty} \sum_{n=-\infty}^{\infty} V_{mn} e^{-j(G_m + \alpha)x} e^{-j(G_n + \beta)y} \\ w(x, y) = \sum_{m=-\infty}^{\infty} \sum_{n=-\infty}^{\infty} W_{mn} e^{-j(G_m + \alpha)x} e^{-j(G_n + \beta)y} \end{cases}, \tag{8}$$

where (α, β) is a Bloch wave vector and $\mathbf{G}_{mn} = (G_m, G_n)$ is the reciprocal-lattice vector of the mn^{th} plane wave, in which $G_m = 2m\pi/a_1$ and $G_n = 2n\pi/b_1$. Substitution of Equations (6)–(8) into Equation (5) yields

$$\begin{cases} (K_{11}U_{mn} + K_{12}V_{mn} + K_{13}W_{mn}) - \omega^2(M_{11}U_{mn} + M_{12}V_{mn} + M_{13}W_{mn}) = 0 \\ (K_{21}U_{mn} + K_{22}V_{mn} + K_{23}W_{mn}) - \omega^2(M_{21}U_{mn} + M_{22}V_{mn} + M_{23}W_{mn}) = 0 \\ \left(K_{31}U_{mn} + K_{32}V_{mn} + K_{33}W_{mn} + \frac{k_R}{S} \sum_{p=-M}^M \sum_{q=-N}^N W_{pq} - \frac{k_R}{S} w_{R0} \right) \\ \quad - \omega^2(M_{31}U_{mn} + M_{32}V_{mn} + M_{33}W_{mn}) = 0 \\ \left(-k_R \sum_{p=-M}^M \sum_{q=-N}^N W_{pq} + k_R w_{R0} \right) - \omega^2(m_R w_{R0}) = 0 \end{cases}, \tag{9}$$

where $S = a_1 b_1$ is the element area and the infinite series in Equations (7) and (8) are truncated to $-M \leq m, s \leq M$ and $-N \leq n, t \leq N$. The term w_{R0} is the displacement of the mass block of the resonator located at $(x = 0, y = 0)$. The expressions of K_{ij} and M_{ij} ($i, j = 1, 2, 3$) are defined in Equations (A10)–(A27) in Appendix A. After some manipulations, Equation (9) can be written in matrix form as

$$[\mathbf{K}(\alpha, \beta) - \omega^2 \mathbf{M}(\alpha, \beta)] \Phi = 0, \tag{10}$$

where $\Phi = [\mathbf{U} \ \mathbf{V} \ \mathbf{W} \ w_{R0}]^T$, $\mathbf{U} = [U_{mn}]_{1 \times [(2M+1) \times (2N+1)]}$, $\mathbf{V} = [V_{mn}]_{1 \times [(2M+1) \times (2N+1)]}$, and $\mathbf{W} = [W_{mn}]_{1 \times [(2M+1) \times (2N+1)]}$. For each given Bloch wave vector $\mathbf{k} = (\alpha, \beta)$, the characteristic frequencies can be determined by Equation (10). By sweeping \mathbf{k} in the directions of ΓX ($\alpha : 0 \rightarrow \pi/a_1, \beta : 0$), ΓM ($\alpha : \pi/a_1, \beta : 0 \rightarrow \pi/a_2$), and $\Gamma \Gamma$ ($\alpha : \pi/a_1 \rightarrow 0, \beta : \pi/a_2 \rightarrow 0$) in the first Brillouin zone (see Figure 1b), the dispersion relationship between wave number and frequency can be obtained, from which the band-gap is then identified.

2.2.2. Sound Radiation

In an infinite LR sandwich plate with wave vector $\mathbf{k} = (k_x, k_y)$, the displacement functions can be assumed as

$$\begin{bmatrix} u & v & w \end{bmatrix} = \begin{bmatrix} U & V & W \end{bmatrix} e^{-jk_x x} e^{-jk_y y}, \tag{11}$$

where $k_x = k_p \cos \varphi$, $k_y = k_p \sin \varphi$, and $k_p = \sqrt{k_x^2 + k_y^2}$ is the structural wave number. The situation of free vibration is considered here to determine the relationship between k_p and frequency. Substitution of Equation (11) into Equations (5) and (6) yields

$$\begin{bmatrix} a_{11}k_p^2 + a_{12} & a_{13}k_p^2 & a_{14}k_p & 0 \\ a_{21}k_p^2 & a_{22}k_p^2 + a_{23} & a_{24}k_p & 0 \\ a_{31}k_p & a_{32}k_p & a_{33}k_p^4 + a_{34}k_p^2 + a_{35} & a_{36} \\ 0 & 0 & a_{41} & a_{42} \end{bmatrix} \begin{bmatrix} U \\ V \\ W \\ w_{R0} \end{bmatrix} = 0, \tag{12}$$

where the coefficients a_{ij} are expressed as a function of frequency, which are defined in Equations (A28)–(A43) in Appendix A. By calculating the matrix determinant of Equation (12), the dispersion equation can be obtained as

$$k_p^8 + \varepsilon_6 k_p^6 + \varepsilon_4 k_p^4 + \varepsilon_2 k_p^2 + \varepsilon_0 = 0, \tag{13}$$

where $\varepsilon_0, \varepsilon_2, \varepsilon_4$, and ε_6 can be calculated with Equations (A44)–(A48) defined in Appendix A. As can be seen in Equation (13), each frequency corresponds to four pairs of conjugate wave numbers, with two of them related to x -wise and y -wise in-plane waves and the other two related to z -wise flexural waves. The far-field sound radiation is strongly related to flexural waves instead of in-plane waves. Further study shows that, for the flexural waves, only one pair corresponds to the propagating waves and the other corresponds to the evanescent (near-field) waves. The waves considered in the theoretical model are in sinusoidal form distributed in the whole infinite structure as shown in Equation (11) instead of point-excited situation, in order to minimize the effect of near-field effect. For the sinusoidal wave form, the sound pressure generated by evanescent wave attenuates rapidly from near surface to far-away sound field, and the sound pressure only exists near the plate surface. In addition, the sound pressure is out of phase with the plate velocity, resulting that there's little sound power radiated from evanescent wave. For the finite sandwich structure in the next subsection, the present model is restricted to lightly damped situation and light-fluid acoustic medium so that the effect of near-field effect can be reasonably ignored. In order to make the theoretical model not too complex, the effects of evanescent flexural waves are ignored in the following analysis.

It is well known that the Helmholtz wave equation in a Cartesian coordinate system is expressed as

$$\frac{\partial^2 p}{\partial x^2} + \frac{\partial^2 p}{\partial y^2} + \frac{\partial^2 p}{\partial z^2} - k_{ac}^2 p = 0, \tag{14}$$

where $k_{ac} = \omega/c$ is the acoustic wave number and c is sound velocity in the surrounding acoustic medium. The sound pressure solution of Equation (14) has the form of $p = p_0 e^{-jk_x x} e^{-jk_y y} e^{-jk_z z}$, substitution of which into Equation (14) yields $k_x^2 + k_y^2 + k_z^2 = k_{ac}^2$. Thus, the transverse acoustic wave number can be expressed as $k_z = \pm \sqrt{k_{ac}^2 - k_p^2}$. The continuity condition for normal velocity at the interface between the plate surface and acoustic medium states that

$$\hat{v} = -\frac{1}{j\omega\rho_0} \frac{\partial p}{\partial z} \Big|_{z=0'} \tag{15}$$

where ρ_0 is the density of the acoustic medium and $\hat{v} = -j\omega w$ is the normal velocity of the plate. After some manipulations, the sound radiation efficiency of an infinite LR sandwich plate is given by

$$\sigma_{\text{inf}} = \sqrt{\frac{k_{ac}^2}{k_{ac}^2 - k_p^2}} \tag{16}$$

where k_p is calculated using Equation (13) at a given frequency. Thus, the radiation efficiency can be finally obtained as a function of frequency.

2.3. Vibro-Acoustic Formulation of a Finite Periodic Structure

An LR sandwich plate with a simply-supported boundary condition is placed in an infinite rigid baffle, which is shown in Figure 2. A harmonic point force is applied on the plate. As the acoustic medium chosen in this paper is air (a light fluid), the effects of fluid load by the acoustic medium on the structure are neglected.

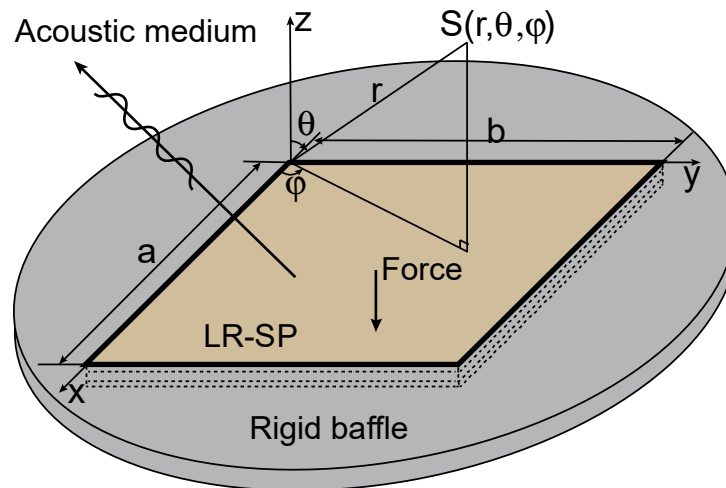


Figure 2. Schematic of a finite locally resonant sandwich plate (LR-SP) baffled in an infinite rigid baffle.

For an LR sandwich plate with a simply-supported boundary condition, the displacements can be written as

$$\begin{cases} u(x, y) = \sum_{m=1}^{\infty} \sum_{n=1}^{\infty} \bar{U}_{mn} \cos(k_m x) \sin(k_n y) \\ v(x, y) = \sum_{m=1}^{\infty} \sum_{n=1}^{\infty} \bar{V}_{mn} \sin(k_m x) \cos(k_n y) \\ w(x, y) = \sum_{m=1}^{\infty} \sum_{n=1}^{\infty} \bar{W}_{mn} \sin(k_m x) \sin(k_n y) \end{cases} \quad (17)$$

where $k_m = m\pi/a$ and $k_n = n\pi/b$. Substituting Equation (17) into Equations (5) and (6), and considering the orthogonality of trigonometric functions yield

$$\begin{cases} (\bar{K}_{11}\bar{U}_{mn} + \bar{K}_{12}\bar{V}_{mn} + \bar{K}_{13}\bar{W}_{mn}) - \omega^2(\bar{M}_{11}\bar{U}_{mn} + \bar{M}_{12}\bar{V}_{mn} + \bar{M}_{13}\bar{W}_{mn}) = 0 \\ (\bar{K}_{21}\bar{U}_{mn} + \bar{K}_{22}\bar{V}_{mn} + \bar{K}_{23}\bar{W}_{mn}) - \omega^2(\bar{M}_{21}\bar{U}_{mn} + \bar{M}_{22}\bar{V}_{mn} + \bar{M}_{23}\bar{W}_{mn}) = 0 \\ \left(\begin{array}{l} \bar{K}_{31}\bar{U}_{mn} + \bar{K}_{32}\bar{V}_{mn} + \bar{K}_{33}\bar{W}_{mn} \\ + \frac{4k_R}{ab} \sum_{p=1}^M \sum_{q=1}^N \sum_{s=1}^S \sum_{t=1}^T \chi_{mn} \chi_{pq} \bar{W}_{pq} \\ - \frac{4k_R}{ab} \sum_{s=1}^S \sum_{t=1}^T \chi_{mn} w_{Rst} \end{array} \right) - \omega^2(\bar{M}_{31}\bar{U}_{mn} + \bar{M}_{32}\bar{V}_{mn} + \bar{M}_{33}\bar{W}_{mn}) = F_{mn} \\ \left(-k_R \sum_{p=1}^M \sum_{q=1}^N \chi_{pq} \bar{W}_{pq} + k_R w_{Rst} \right) - \omega^2(m_R w_{Rst}) = 0 \end{cases} \quad (18)$$

where $\chi_{mn} = \sin(k_m x_s) \sin(k_n y_t)$, $\chi_{pq} = \sin(k_p x_s) \sin(k_q y_t)$, and w_{Rst} is the displacement of the mass block of the st^{th} resonator. For a point force excitation applied at position (x_0, y_0) , the force term is written as $F_{mn} = \frac{4F_0}{ab} \sin(k_m x_0) \sin(k_n y_0)$. The expressions of \bar{K}_{ij} and \bar{M}_{ij} ($i, j = 1, 2, 3$) are defined in

Equations (A49)–(A66) in Appendix A. After further manipulations, Equation (18) can be written in matrix form as

$$[\bar{\mathbf{K}} - \omega^2 \bar{\mathbf{M}}] \bar{\boldsymbol{\Phi}} = \mathbf{F}, \tag{19}$$

where $\bar{\boldsymbol{\Phi}} = [\bar{\mathbf{U}} \ \bar{\mathbf{V}} \ \bar{\mathbf{W}} \ \bar{\mathbf{W}}_{\mathbf{R}}]^T$, $\bar{\mathbf{U}} = [\bar{U}_{mn}]_{1 \times (M \times N)}$, $\bar{\mathbf{V}} = [\bar{V}_{mn}]_{1 \times (M \times N)}$, $\bar{\mathbf{W}} = [\bar{W}_{mn}]_{1 \times (M \times N)}$, $\bar{\mathbf{W}}_{\mathbf{R}} = [\bar{W}_{Rst}]_{1 \times (S \times T)}$, $\mathbf{F} = [0 \ 0 \ \mathbf{F}_w \ 0]$, and $\mathbf{F}_w = [F_{mn}]_{1 \times (M \times N)}$. The infinite series in Equation (17) are truncated to $1 \leq m \leq M$ and $1 \leq n \leq N$. Then the modal frequencies and modal shapes can be obtained by setting \mathbf{F} as zero, and the modal coefficient $\bar{\boldsymbol{\Phi}}$ can be determined by setting \mathbf{F} as nonzero. After $\bar{\boldsymbol{\Phi}}$ is known, the displacement response of the LR sandwich plate can finally be determined using Equation (17), from which the transverse velocity can be obtained as $\hat{v}(x, y) = \sum_{m=1}^{\infty} \sum_{n=1}^{\infty} \hat{V}_{mn} \sin(k_m x) \sin(k_n y)$, where $\hat{V}_{mn} = -j\omega \bar{W}_{mn}$. The spatially averaged mean square velocity can be calculated as

$$\langle \hat{v}^2 \rangle = \sum_{m=1}^M \sum_{n=1}^N \frac{1}{8} \hat{V}_{mn} \hat{V}_{mn}^*, \tag{20}$$

where the superscript asterisk denotes the complex conjugate of a variable. According to the Rayleigh integral, the acoustic pressure p at the far-field observation point (r, θ, φ) can be written in terms of the plate-surface velocity $\hat{v}(x, y)$

$$p(r, \theta, \varphi) = \frac{jk_{ac}c\rho_0}{2\pi} \int_0^a \int_0^b \frac{\hat{v}(x, y) e^{-jkr}}{r} dy dx. \tag{21}$$

Substitution of Equation $\hat{v}(x, y) = \sum_{m=1}^{\infty} \sum_{n=1}^{\infty} \hat{V}_{mn} \sin(k_m x) \sin(k_n y)$ into Equation (21) gives

$$p(r, \theta, \varphi) = \sum_{m=1}^{\infty} \sum_{n=1}^{\infty} \hat{V}_{mn} T_{mn}(r, \theta, \varphi). \tag{22}$$

Here

$$T_{mn}(r, \theta, \varphi) = jk_{ac}\rho_0c \frac{e^{-jkr}}{2\pi r} \frac{ab}{mn\pi^2} \frac{(-1)^m e^{-j\tau_x} - 1}{(\tau_x/m\pi)^2 - 1} \frac{(-1)^n e^{-j\tau_y} - 1}{(\tau_y/n\pi)^2 - 1}, \tag{23}$$

where $\tau_x = ka \sin \theta \cos \varphi$ and $\tau_y = kb \sin \theta \sin \varphi$. Thus, the total acoustic power radiated from the LR sandwich plate can be obtained by integrating sound intensity over a far-field hemisphere with radius r

$$\Pi = \int_0^{2\pi} \int_0^{\pi/2} \frac{|p(r, \theta, \varphi)|^2}{2\rho_0c} r^2 \sin \theta d\theta d\varphi. \tag{24}$$

Substituting Equation (22) into Equation (24) gives

$$\Pi = \sum_{m=1}^{\infty} \sum_{n=1}^{\infty} \sum_{p=1}^{\infty} \sum_{q=1}^{\infty} \Pi_{mnpq}, \tag{25}$$

where Π_{mnpq} is the acoustic power radiated by mode (m, n) due to the vibration of mode (p, q) , and it is given by

$$\Pi_{mnpq} = \hat{V}_{mn} \hat{V}_{pq}^* \int_0^{2\pi} \int_0^{\pi/2} \frac{T_{mn}(r, \theta, \varphi) T_{pq}^*(r, \theta, \varphi)}{2\rho_0c} r^2 \sin \theta d\theta d\varphi. \tag{26}$$

Thus, the modal radiation efficiency can be expressed as

$$\sigma_{mnpq} = \frac{\Pi_{mnpq}}{\frac{1}{8}\rho_0cab\hat{V}_{mn}\hat{V}_{pq}^*} = \int_0^{2\pi} \int_0^{\pi/2} \frac{4}{\rho_0^2c^2ab} T_{mn}(r, \theta, \varphi) T_{pq}^*(r, \theta, \varphi) r^2 \sin \theta d\theta d\varphi, \tag{27}$$

and the total average radiation efficiency of the LR sandwich plate is given by

$$\sigma = \frac{\Pi}{\frac{1}{2}\rho_0cab\langle\hat{v}^2\rangle} = \frac{\sum_{m=1}^{\infty} \sum_{n=1}^{\infty} \sum_{p=1}^{\infty} \sum_{q=1}^{\infty} \hat{V}_{mn} \hat{V}_{pq}^* \sigma_{mnpq}}{\sum_{m=1}^{\infty} \sum_{n=1}^{\infty} \hat{V}_{mn} \hat{V}_{mn}^*}. \tag{28}$$

From Equation (28), when the modal vibration coefficient and the modal radiation efficiency are obtained, the sound radiation power can be finally determined to illustrate the sound radiation performance caused by the coupling effect between resonators and a sandwich plate.

3. Results and Discussion

The dimensions of a unit element of an LR sandwich plate are set as $a_1 = b_1 = 100$ mm, $h_f = 2$ mm, $h_c = 16$ mm, and $r_o = 15$ mm. The surface layer is made of aluminum with Young’s modulus $E_f = 77.6$ GPa, density $\rho_f = 2730$ kg/m³, and Poisson’s ratio $\nu_f = 0.35$, while the core layer is made of foam with shear modulus $G_c = 0.05$ GPa and density $\rho_{c0} = 110$ kg/m³. The cylindrical mass of the resonator is made of lead with radius $r_i = 12$ mm, height $h_{cR} = 6$ mm, and density $\rho_R = 11600$ kg/m³. Thus, the mass of the resonator is calculated as 0.0315 kg, which is 25% of the mass of a unit sandwich element without a resonator. The resonator is tuned to 1000 Hz with a spring stiffness of $k_R = 1.2436 \times 10^6$ N/m. In the following analysis, the above parameters are kept unchanged unless otherwise stated.

3.1. Band-Gap Property

The dispersion curves of an infinite LR sandwich plate are calculated using the theory derived in Section 2.2.1. At the same time, the dispersion curves of an infinite homogeneous sandwich plate with the same dimensions and same materials are also discussed for comparison purposes.

The dispersion curves of these two structures are shown together in Figure 3. It can be seen that, for the homogeneous sandwich plate, each frequency is always related to a wave number in the ΓX direction and a wave number in the ΓM direction in the irreducible Brillouin zone, which means that propagating modes are allowed at any frequency. However, for the LR sandwich plate, there are some frequencies that are not related to any wave number in the ΓX direction. Two directional band-gaps (DBG) along the ΓX direction and one complete band-gap (CBG) are observed in the figure with band-gap frequencies of 825–1032 Hz and 1476–1677 Hz for the two DBGs and 868–1032 Hz for the CBG, respectively. Further analysis shows that the first DBG located near the resonance of the resonator acts as a resonance gap, which is caused by the LR effect; and the second DBG is a Bragg gap, which is caused by wave scattering at periodic discontinuities and is affected significantly by the lattice constant. These two types of band-gaps can be identified by comparing the modal shape of each dispersion curve. The Bragg gap can also be identified by the Bragg frequency f_B (the lower frequency edge of a Bragg gap), where the wavelength is twice as that of the lattice constant, and it can be determined by solving the transcendental equation $k_P(f_B) = \pi/a_1$, where f_B is calculated to be 1476 Hz.

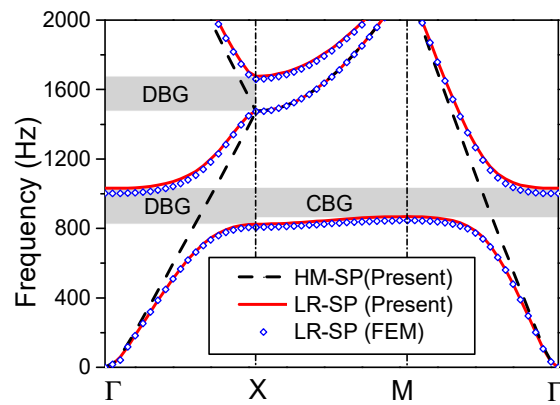


Figure 3. Dispersion curves of a locally resonant sandwich plate (LR-SP) and a homogeneous sandwich plate (HM-SP). (DBG—directional band-gap; CBG—complete band-gap.).

In a finite periodic structure, the DBGs along the ΓX direction can only exist in a situation with symmetric excitation, whereas the CBG is more general, where a wave from any direction can be attenuated and the sound radiation from a finite structure is affected significantly by the CBG instead of the DBG. Thus, this research will focus on the CBG and the term “band-gap” used in the next sections will refer to the CBG.

The theoretical formulations are validated using a finite-element-method (FEM) numerical model based on the COMSOL Multiphysics software. Shown in Figure 4a is a unit element, which mainly consists of the bottom sandwich part and the top mass-block part. The dimensions and material properties of the sandwich part are the same as that shown in the beginning of Section 3, except that the density of the core is modified to be 102.2 kg/m^3 as the core layer is considered as homogeneous in the FEM model. The mass of the top mass-block part is set to be 0.0315 kg and its Young’s modulus is set to be as large as $1 \times 10^{15} \text{ Pa}$ so that the block could be considered as a rigid body. A connection function called “elastic layer” in COMSOL is added in the FEM modal between the bottom sandwich part and the top mass-block part, so that the two parts are elastically connected. The spring stiffness of the “elastic layer” is set to be $k_R = 1.2436 \times 10^6 \text{ N/m}$, which is the same as that described in the beginning of Section 3. The meshing model is shown in Figure 4b with the element size set as small as 2 mm for the purpose of satisfying the adequate meshing resolution at the highest frequency 2000 Hz .

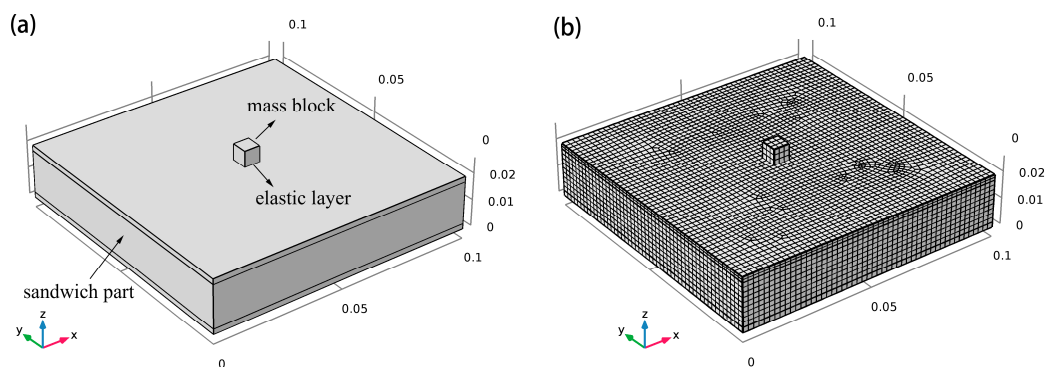


Figure 4. (a) The numerical structure model and (b) its meshing model.

In order to obtain the band-gap properties, the Bloch–Floquet periodic conditions are applied at two in-plane (both x -wise and y -wise) directions in the FEM model, which are represented by a Bloch wave vector $\mathbf{k} = (\alpha, \beta)$. By sweeping \mathbf{k} in x -wise direction ($\alpha : 0 \rightarrow \pi/a_1, \beta : 0$), y -wise direction ($\alpha : \pi/a_1, \beta : 0 \rightarrow \pi/a_2$), and corner-to-corner direction ($\alpha : \pi/a_1 \rightarrow 0, \beta : \pi/a_2 \rightarrow 0$), the dispersion relationship between wave number and frequency can be obtained by further applying characteristic frequency analysis in the simulation software.

The dispersion curves calculated from the numerical model are shown together with the results from the present analytical model in Figure 3. It can be seen that the results from the present model have an excellent agreement with those from the FEM model, which shows that the solutions of the present analytical model have sufficient precision.

3.2. Vibration Response of a Finite LR Sandwich Plate

The vibration response of a finite LR sandwich plate with a simply-supported boundary is further studied to illustrate the band-gap phenomenon of vibration in a practical finite structure. The examined structure is composed of 10×8 cells (1×0.8 m) with cell parameters the same as those shown in the previous sub-section. A transverse point force is applied at position (0.1, 0.1 m) with a harmonic form and the whole structure is structurally damped with a damping loss factor of $\eta = 0.002$.

The root-mean-square velocity averaged over the plate surface and each modal contribution of an LR sandwich plate are shown in Figure 5a, together with the results of an equivalent homogeneous sandwich plate shown in Figure 5b. Comparison of Figures 5a and 3 shows that the band-gaps of an infinite periodic LR sandwich plate are coincident with the response valleys of a finite periodic structure. In the band-gap frequency region (868–1032 Hz), the vibration of the LR sandwich plate is significantly reduced compared with that of a homogeneous sandwich plate.

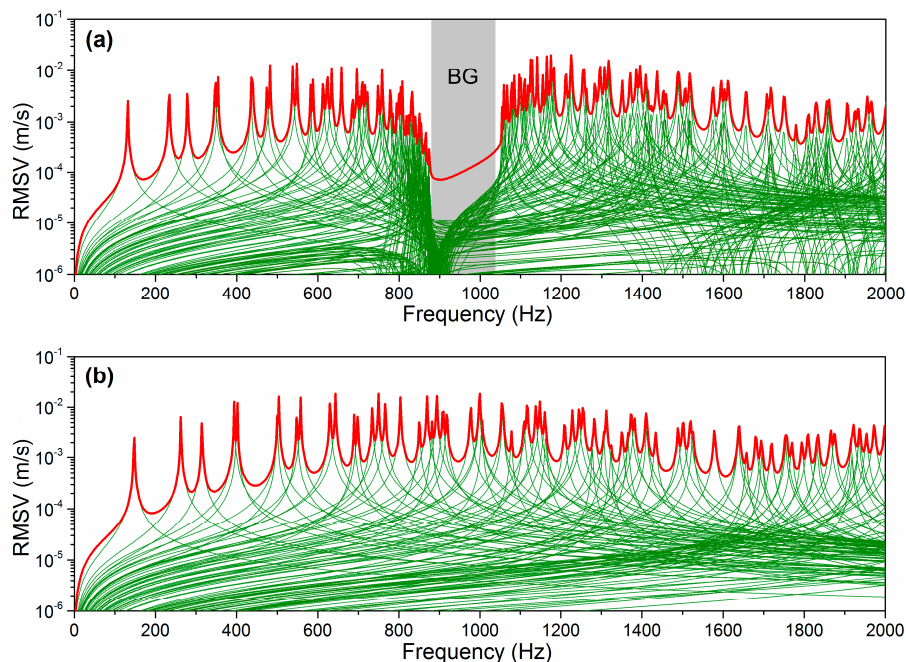


Figure 5. Root-mean-square velocity (RMSV) averaged over the plate surface and corresponding modal contributions in (a) a locally resonant sandwich plate and (b) a homogeneous sandwich plate. (BG—band-gap.)

In fact, the reduction of vibration in the band-gap can be explained by the effects of the resonators on each vibration mode. As can be observed in Figure 5a, all the modal responses are significantly affected by periodic resonators, with a weak response contribution in the band-gap but strong contribution outside of the band-gap. Further explanation is given in Figure 6, where three specific modes (mode (2, 3), mode (5, 4), and mode (5, 6)) are given for both the LR and homogeneous sandwich plates. It is observed that, for the homogeneous sandwich plate, only one peak appears in the curve, which corresponds to the flexural vibration mode. However, when the resonators are introduced to the sandwich plate, a new peak related to the resonator vibration mode is generated as a result of vibration coupling between the resonator and base plate. In addition, the flexural mode of the homogeneous sandwich plate is shifted to a lower or higher frequency in the LR sandwich plate.

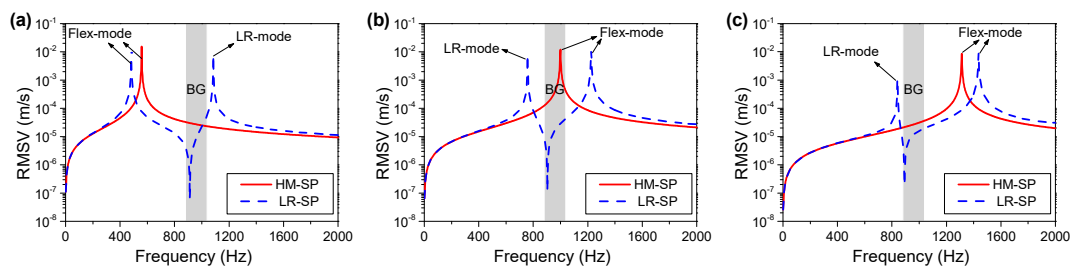


Figure 6. Comparison of modal contributions for a homogeneous sandwich plate (HM-SP) and a locally resonant sandwich plate (LR-SP) for (a) mode (2, 3), (b) mode (5, 4), and (c) mode (5, 6). (Flex-mode—flexural vibration mode; LR-mode—resonator vibration mode.).

Further observation of Figures 5 and 6 shows that these two modal frequencies in the LR sandwich plate are always set apart by the band-gap, with one mode positioned at the left side and the other at the right side, and that no mode exists in the band-gap. This phenomenon is also revealed through modal analysis of an LR sandwich plate and a homogeneous sandwich plate, and their modal frequencies are shown in Figure 7. For the homogeneous sandwich plate, the modes may be positioned at any frequency based on the dimensions and boundary conditions of the finite structure. However, for a homogenous sandwich plate, when resonators are introduced the modal frequencies positioned within the band-gap are shifted to the left side or right side of the band-gap. As a result, vibration modes are not allowed in the band-gap of the LR sandwich plate. Thus, the vibration in the band-gap can be reduced.

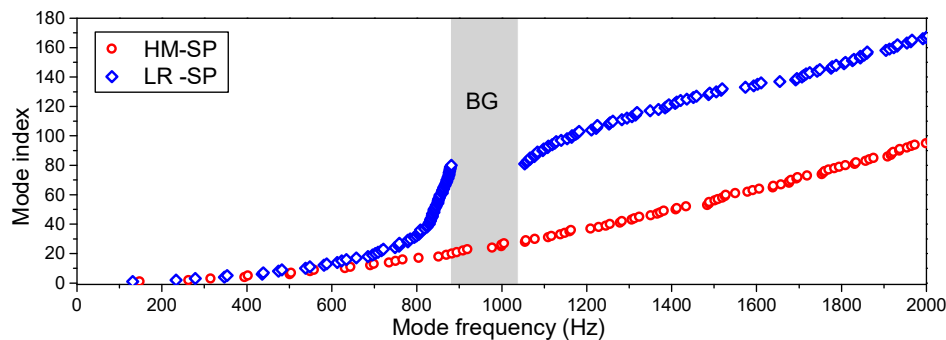


Figure 7. Comparison of modal frequencies for a homogeneous sandwich plate (HM-SP) and a locally resonant sandwich plate (LR-SP).

3.3. Radiation Efficiency of an Infinite LR Sandwich Plate

It was found from the above analysis that periodic resonators can improve the vibration performance of an LR sandwich plate in the band-gap frequency region. As the sound radiation ultimately depends on vibration, the radiation performance will also be affected significantly. In this subsection, the radiation efficiency of an infinite LR sandwich plate is examined here to reveal the effects of periodic resonators on radiation characteristics.

Shown in Figure 8a–c are the structural wave number k_p , acoustic wave number k_{ac} , transverse acoustic wave number $k_{zr} = \text{real}(\sqrt{k_{ac}^2 - k_p^2})$, and radiation efficiency σ_{inf} of an infinite homogeneous sandwich plate (HM-SP) in Figure 8a, an infinite LR sandwich plate (LR-SP) with the resonator tuned at $f_R = 1000$ Hz in Figure 8b, and an infinite homogeneous sandwich plate with the LR mass added to the core layer (HM-SP2) in Figure 8c. The difference between HM-SP and HM-SP2 is that the mass of resonator is added to the core layer in HM-SP2 in order to examine the effects of increase of weight due to periodic resonators on radiation properties, thus the weight of the structure of HM-SP2 keeps the same as that of the structure of LR-SP. It is well known that, in an infinite structure, sound radiates efficiently only in situations where the phase speed of a structural wave exceeds the speed of sound in

the surrounding medium ($c_P > c_{ac}$, $k_P < k_{ac}$). Thus, k_{zr} can be considered as an indicator of whether a wave with a specific frequency radiates efficiently or not, that is, a wave radiates efficiently when k_{zr} exceeds zero and inefficiently when k_{zr} equals zero. For a homogeneous structure, the frequency that satisfies $k_P = k_{ac}$ is generally called the coincidence frequency, where vibration energy may transform to sound radiation power most efficiently and the corresponding radiation efficiency tends to infinity.

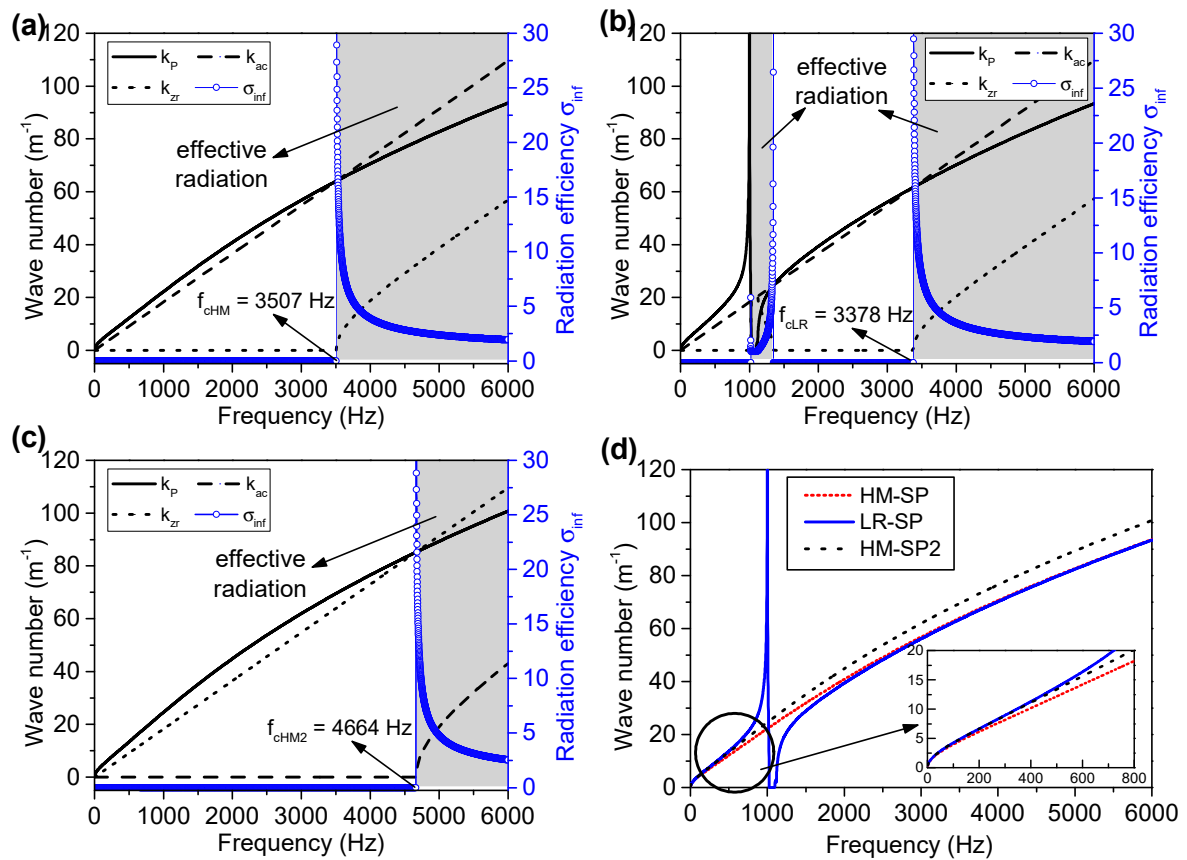


Figure 8. Wave numbers and radiation efficiencies of (a) an infinite homogeneous sandwich plate (HM-SP), (b) an infinite locally resonant sandwich plate (LR-SP), and (c) an infinite homogeneous sandwich plate with the LR mass added to the core layer (HM-SP2). (d) The comparison of structural wave numbers among the above three plates.

As shown in Figure 8a, the coincidence frequency of the HM-SP is $f_{cHM} = 3507$ Hz. With the increase in frequency, the radiation efficiency σ_{inf} stays constant at zero below f_{cHM} , then reaches infinity at f_{cHM} , and finally decreases from infinity to unity above f_{cHM} . Thus, the effective radiation region begins at 3507 Hz, where vibration energy can be radiated into the acoustic medium efficiently. In Figure 8c for the structure of HM-SP2, the variation trends of wave numbers and radiation efficiency keep the same as that in HM-SP, except that the coincidence frequency changes from 3507 Hz to 4666 Hz because of the increased weight in the core layer. Thus, the effective radiation region for HM-SP2 begins at 4664 Hz.

However, the case of the LR sandwich plate differs from that of the homogeneous sandwich plate. As is shown in Figure 8b, the acoustic wave number k_{ac} is the same as in the homogeneous sandwich plate, while the structural wave number k_P varies significantly near the band-gap region (compare Figure 8a,b). With the increase in frequency, k_P first increases gradually from zero to infinity over 0–1000 Hz, and then decreases sharply from infinity to zero over 1001–1026 Hz, then remains unchanged at zero over 1027–1097 Hz, and finally increases from 1098 Hz to infinity. As k_{zr} is calculated from k_{ac} and k_P , it is also significantly affected by the resonators near the band-gap frequency region

(868–1032 Hz). It is noticed in Figure 8b that the coincidence frequency becomes $f_{cLR} = 3378$ Hz, which is 129 Hz lower than that of the structure of HM-SP. Furthermore, because of the variation of k_p , k_{zr} becomes positive from 1018 to 1346 Hz, which corresponds to effective sound radiation. Thus, affected by k_{zr} , two effective radiation regions are formed, namely 1018–1346 Hz and 3378 Hz–∞. The first one is the resonator-induced effective radiation region, which is located above the band-gap (868–1032 Hz) with a small zone overlapping (1018–1032 Hz). Thus, for waves with frequencies close above the band-gap, acoustic radiation may be enhanced due to the effective radiation region.

As the radiation efficiency is strongly related to the structural wave number k_p , the structural wave numbers of HM-SP, LR-SP, and HM-SP2 are compared to further examine the radiation properties in Figure 8d. As shown in the figure, in the lower frequencies between 0 Hz to approximately 600 Hz, the structural wave number k_p of LR-SP nearly coincidence with that of HM-SP2. It is noticed that these above two structures have the same weight, thus the increased weight introduced by periodic resonators have some effect on the radiation. In contrast to lower frequencies, in the higher frequencies between approximately 2.5 to 6 kHz, k_p of LR-SP nearly coincides with that of HM-SP, inducing that the weight introduced by periodic resonators have little effect on the radiation properties in high frequencies.

It is noticed from the comparison between Figure 8a,b that the effects of periodic resonators on the sound radiation of an infinite sandwich plate mainly contain two terms. The first is the decrease in coincidence frequency from 3507 to 3378 Hz, and the second is the newly generated effective radiation region. Thus, the total effective radiation region is actually enlarged, and the ineffective radiation region in a homogeneous sandwich plate may be changed to an effective radiation region in an LR sandwich plate. Although the vibration in the band-gap is reduced, sound radiation in other frequencies may be enhanced. Therefore, care should be taken when designing a band-gap for noise-reduction purposes as the band-gap design may in fact enlarge the effective radiation region.

In fact, the variation of acoustic radiation can be physically explained by the normalized effective mass m_e of an LR sandwich plate, which is expressed as

$$m_e = 1 + \frac{m_R k_R}{m_b (k_R - \omega^2 m_R)}, \tag{29}$$

where m_b is the mass of a unit element of the base sandwich plate. As shown in Figure 8, radiation efficiency is strongly dependent on the structural wave number k_p , thus m_e and k_p are shown together in Figure 9 for further analysis. It is observed that, with the increase in frequency, m_e increases from 1.25 to infinity over 0–1000 Hz, then increases from minus infinity to approximately unity (but always less than unity) between 1000 and 6000 Hz. In the lower frequencies, the limit of m_e is 1.25, which is exactly the effective mass of the structure of HM-SP2. In the higher frequencies, m_e tends to unity, which is exactly the effective mass of the structure of HM-SP. This phenomenon is the same as that observed in Figure 8b. It can also be observed that the effective mass is disconnected at 1000 Hz (the resonance frequency of the resonator). By comparing the two curves in Figure 9, it is found that k_p varies synchronously with m_e , and the position where m_e reaches its maximum is also the position of the maximum of k_p . This phenomenon can be simply comprehended by referring to a homogenous single-layer plate, whose structural wave number is proportional to the fourth-root of the material density, that is, $k_p = \sqrt[4]{\omega^2 \rho h / D}$. Thus, k_p increases with increasing density/mass and decreases with decreasing density/mass.

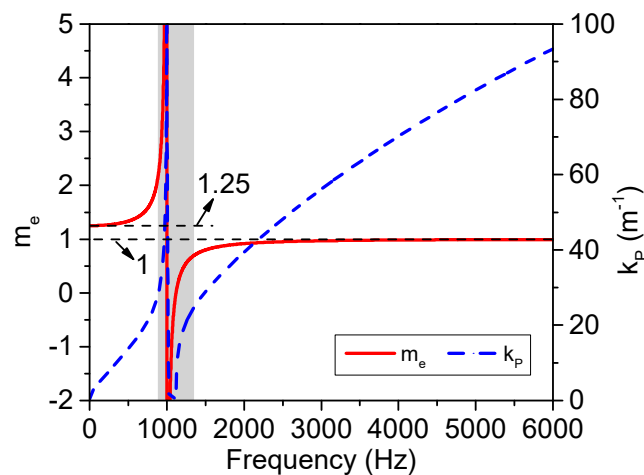


Figure 9. Normalized effective mass and structural wave number of a locally resonant sandwich plate.

In addition, the radiation efficiency is affected by the structural wave number as can be inferred from Equation (16). Thus, it can be concluded that the special radiation performance of the LR sandwich plate shown in Figure 8b is mainly caused by the variation in effective mass. The break in effective mass at 1000 Hz causes k_p to have a sudden drop close above 1000 Hz, resulting in k_p becoming less than k_{ac} , which should not occur in a homogeneous sandwich plate below the coincidence frequency. Affected by this variation, a new resonator-induced effective radiation region (1018 Hz–1346 Hz) is then generated. The decrease in coincidence frequency from 3507 Hz to 3378 Hz in an LR sandwich plate can also be explained by the effective mass. This is easy to understand by referring to a homogeneous single-layer plate, as the coincidence frequency can be described with an explicit expression, written as $f_c = c^2 \sqrt{\rho h} / 2\pi \sqrt{D}$, where f_c is proportional to the square root of the material density. As the effective mass m_e is less than unity above 1000 Hz, the coincidence frequency is decreased in the LR sandwich plate.

3.4. Acoustic Radiation of a Finite LR Sandwich Plate

As was studied in Section 3.2, the introduction of periodic resonators had significant effects on the vibration response, especially in the band-gap, where vibration response is significantly reduced. This variation in vibration will in turn directly affect the acoustic radiation, owing to the coupling between vibration and acoustic radiation. Thus, it can be inferred that the sound radiation in the band-gap may also be reduced as a result of the great reduction in vibration. However, the sound radiation performance beyond the band-gap cannot be estimated simply from vibration performance, as the sound radiation is also greatly dependent on radiation efficiency, which quantifies how much vibration energy can be transformed to sound radiation energy. Thus, this sub-section examines the radiation efficiency and the final sound radiation power in order to further understand the vibro-acoustic performance of an LR sandwich plate.

The structural model is the same as that used in Section 3.2. After the vibration response is determined, the sound radiation power from this finite LR sandwich plate is then determined using a Rayleigh integral in the far field. The corresponding average radiation efficiency is determined from the modal radiation efficiency σ_{mnpq} and modal velocity response \hat{V}_{mn} using Equation (28). As the radiation surface, structural boundary, and structural size of the homogeneous sandwich plate are the same as those of the LR sandwich plate, the modal radiation efficiencies of both sandwich structures are identical. Therefore, the variation in average radiation efficiency of both sandwich structures is, in effect, due to the variation in the modal velocity response, as shown in Figure 5.

Shown in Figure 10 is a comparison of the radiation efficiencies of homogeneous (σ_{HM}) and LR (σ_{LR}) sandwich plates. It is noticed that the effects of the periodic resonators on radiation efficiency depend

on frequency. In the figure, the whole frequency zone is divided into four parts: zone I (0 Hz– f_{11}), zone II (f_{11} – f_{LR}), zone III (f_{LR} – f_{cLR}), and zone IV (f_{cLR} –6000 Hz), where $f_{11} = 132$ Hz, $f_{LR} = 1000$ Hz, and $f_{cLR} = 3378$ Hz are the fundamental frequency, the resonance frequency of the resonator, and the coincidence frequency of the LR sandwich plate, respectively. Below the fundamental frequency (zone I) and above the coincidence frequency (zone IV), the periodic resonators have little small effect on radiation efficiency and σ_{LR} and σ_{HM} are nearly the same, with σ_{LR} slightly higher than σ_{HM} in zone I and slightly lower in zone IV. Meanwhile, in zone II and zone III, σ_{LR} and σ_{HM} vary significantly and the periodic resonators have a negative effect on radiation efficiency in zone II and a positive effect in zone III. Thus, compared with the homogeneous sandwich plate, the radiation performance of the LR sandwich plate is improved in zone II yet deteriorated in zone III. It is also noticed that, at frequencies close above the band-gap in zone III, σ_{LR} reaches a local maximum of 1.99 at 1158 Hz, which is more than five times that of σ_{HM} . In the frequency band close to 1158 Hz, the LR sandwich plate radiates very efficiently. In fact, this frequency region is simply the resonator-induced effective radiation zone in an infinite LR sandwich plate, which can be found by comparing the radiation efficiency of finite and infinite LR sandwich plates, as shown in Figure 11, where the two shaded regions are the effective radiation zones in an infinite LR sandwich plate.

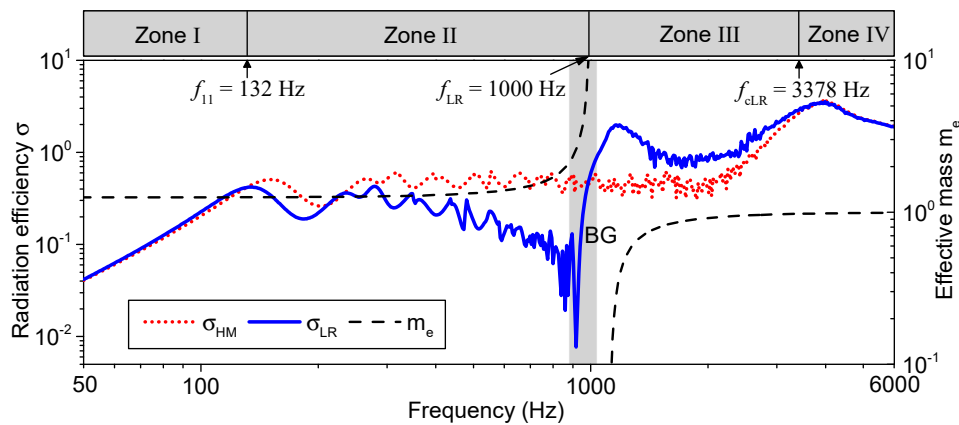


Figure 10. Comparison of radiation efficiencies between a homogeneous sandwich plate and a locally resonant (LR) sandwich plate, together with the normalized effective mass of an LR sandwich plate.

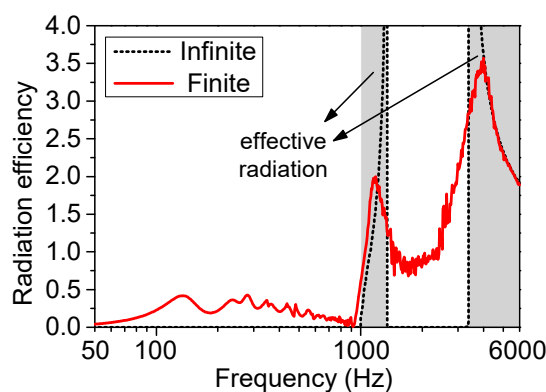


Figure 11. Comparison of radiation efficiencies between finite and infinite locally resonant sandwich plates.

In fact, the variation between σ_{LR} and σ_{HM} can be physically explained by the effective mass and how the mass will affect radiation depends on how the energy is radiated. As can be analyzed from the curves of radiation efficiency, zone I is related to monopole radiation and zones II and III correspond to the so-called corner-mode radiation (from 132 to around 2000 Hz) and edge-mode radiation (from around 2000 to 3378 Hz), where sound radiation is mainly limited at the corner or edge of the plate.

Above the coincidence frequency in zone IV, the finite structure behaves as an infinite structure with regards to sound radiation. The normalized effective mass m_e is shown in Figure 10 to further illustrate the effect of m_e on radiation efficiency.

In zone I, σ_{LR} is mainly contributed to from the first several modes, where the first mode makes the greatest contribution, as it has the greatest modal vibration velocity and also the greatest modal radiation efficiency below the fundamental frequency. Thus, both σ_{HM} and σ_{LR} can be approximately estimated from the radiation efficiency of the first mode, $\sigma_{11} = 4abf^2/c_{ac}^2$, which is the reason it is generally considered as monopole radiation. As shown in this expression, the radiation efficiency is not related to the parameter of mass, and thus the variation in effective mass has little effect on radiation efficiency in zone I. In zone IV, the radiation efficiency of a finite sandwich structure is approximately the same as that of an infinite sandwich structure. Thus, the radiation efficiencies of these two sandwich structures can be expressed as $\sigma_{LR} \approx (1 - f_{cLR}/f)^{-1/2}$ and $\sigma_{HM} \approx (1 - f_{cHM}/f)^{-1/2}$. As m_e is below unity above 1000 Hz, $f_{cLR} < f_{cHM}$, which was analyzed in Sub-Section 3.3. Therefore, at most of the frequencies in zone IV, σ_{LR} is slightly smaller than σ_{HM} . Furthermore, with the increase in frequency, m_e gradually becomes approximately equal to unity, resulting in the radiation efficiency of the LR sandwich plate being nearly the same as that of the homogeneous sandwich plate. In zone II and zone III, for corner-mode and edge-mode radiation, it can be inferred from Equation (25) in [50] that the material density has a negative effect on radiation efficiency. Thus, the increasing mass in zone II induces decreasing radiation efficiency, while the decreasing mass in zone III induces increasing radiation efficiency, especially near the resonance frequency of the resonator.

From the above analysis, it can be concluded that the effect of the periodic resonators on radiation efficiency is due to their effect on the effective mass. The effective mass can be used to indicate which part of the frequency region is acoustically improved and which part is acoustically deteriorated. Thus, when the effective mass of an LR sandwich structure is obtained, the radiation efficiency can be estimated to some degree, which gives a rough prediction of the final radiation performance. This can be important for the band-gap design of an LR sandwich plate.

The sound radiation power of an LR sandwich plate and a homogeneous sandwich plate are shown in Figure 12, together with the radiation efficiency of the LR sandwich plate. The power is expressed in decibels with the reference power selected to be 6.67×10^{-19} W. As shown in the figure, in the band-gap (825–1032 Hz), the acoustic radiation of the LR sandwich plate is reduced significantly with an average attenuation of 31.5 dB compared with that of the homogeneous sandwich plate. This improved acoustic performance is mainly caused by the reduction in vibration, as can be seen from Figure 13, yet it should also be noticed that the reduced radiation efficiency in much of the band-gap also makes a positive contribution to reducing sound radiation. It is interesting to observe that the acoustic performance is significantly improved not only in the band-gap, but also in the frequency region close below the band-gap. As can be calculated from 500 to 868 Hz, the average radiation power of the LR sandwich plate is 8.4 dB lower than that of the homogeneous sandwich plate. In this frequency band, the attenuation is mainly due to the decreased radiation efficiency, which is physically caused by the increased effective mass, as can be seen from Figures 10 and 12. Thus, after the periodic resonators are introduced to the sandwich plate, the acoustic performance is improved both in the band-gap and below the band-gap, due to either the vibration reduction or the decreased radiation efficiency. However, as shown in Figure 12, in the frequency region close above the band-gap, the acoustic radiation is enhanced. From 1060 to 1400 Hz, the average radiation power of the LR sandwich plate is increased by 9.1 dB compared with that of the homogeneous sandwich plate. Most of this frequency band is overlapped with the newly generated effective radiation region (1018–1346 Hz) in an infinite structure, where the radiation efficiency is significantly increased (see Figure 11). Therefore, the increased radiation power close above the band-gap is mainly caused by the increased radiation efficiency, although the vibration response is also slightly increased (see Figure 13).

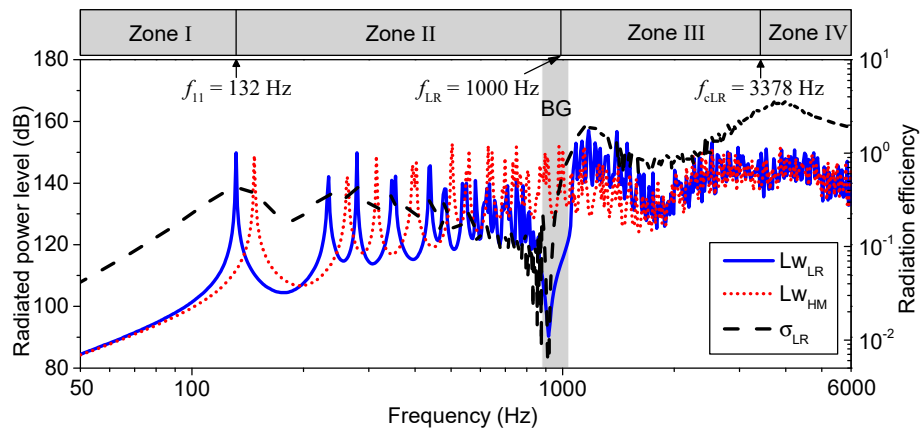


Figure 12. Comparison of sound radiation power between a locally resonant (LR) sandwich plate and a homogeneous sandwich plate, together with the radiation efficiency of an LR sandwich plate.

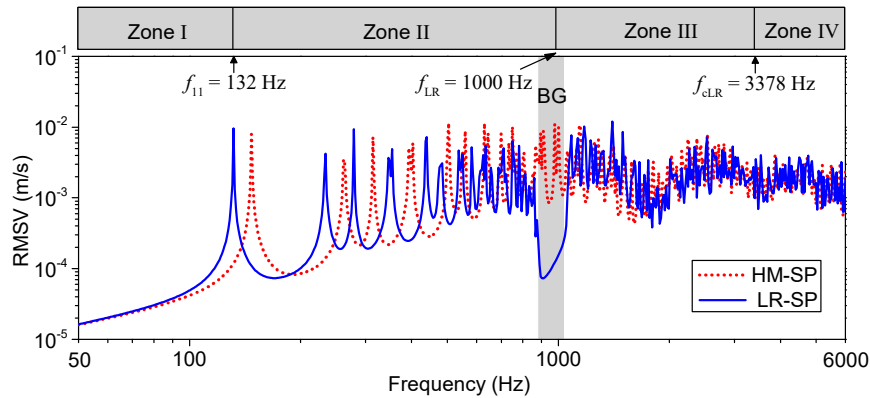


Figure 13. Comparison of root-mean-square velocity (RMSV) between a locally resonant sandwich plate and a homogeneous sandwich plate.

As can be seen in the above results, after periodic resonators are introduced into the sandwich plate, the acoustic performance is improved both in the band-gap and below the band-gap, while the acoustic radiation close above the band-gap is enhanced, owing to both increased radiation efficiency and increased vibration velocity. It is interesting to note that this undesired sound radiation can be suppressed by adding a small damping on the resonator. By doing this, the acoustic performance in the frequency bands above and below the band-gap will both be improved.

In order to make the computation concise, hysteretic damping with damping loss factor η_R is added to the spring of the resonator, with a complex stiffness expressed as $\bar{k}_R = k_R(1 + j\eta_R)$. The sound radiation power of a damped LR sandwich plate with $\eta_R = 0.05$ is shown in Figure 14a. It is observed that the damping of the resonator has a minimal effect on sound radiation below 550 Hz and above 1600 Hz. In the band-gap, the maximal attenuation of radiation is decreased when damping is introduced to the resonator. However, at frequencies close below and close above the band-gap, the sound radiation is significantly reduced compared with that of the undamped LR sandwich plate. As shown in Figure 15, with the increase in damping, the sound radiation becomes increasingly smaller in the frequency ranges of 500–900 Hz and 1050–1600 Hz.

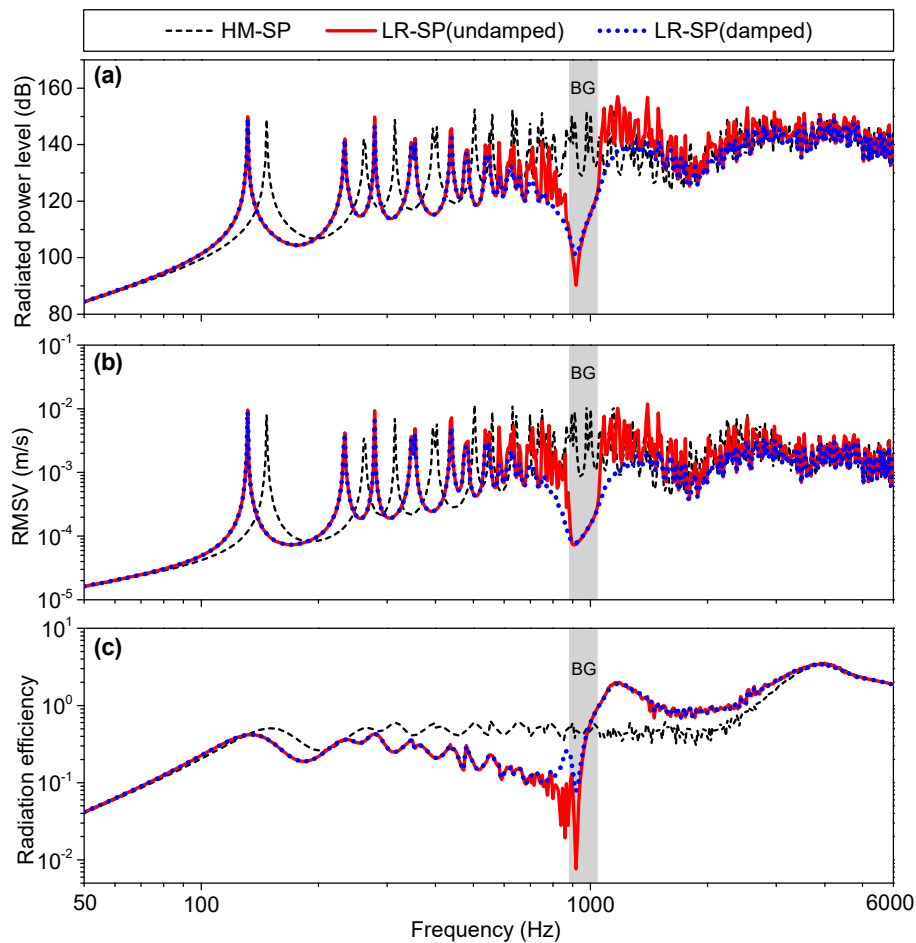


Figure 14. (a) Sound radiation power, (b) root-mean-square velocity (RMSV), and (c) radiation efficiency of a homogeneous sandwich plate (HM-SP) and a locally resonant sandwich plate (LR-SP) with damped and undamped periodic resonators.

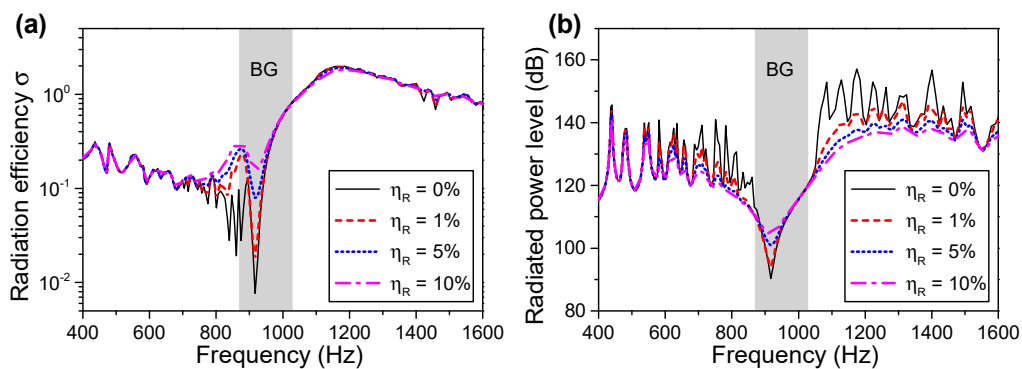


Figure 15. (a) Radiation efficiencies and (b) radiation power of a locally resonant sandwich plate with various damping parameters for the resonator.

Generally speaking, the damping of the resonator broadens the attenuation zone of sound radiation, especially when the sound radiation above the band-gap is also reduced. In much of the attenuation zone, radiation suppression caused by damping of the resonator is mainly due to the effect of damping on the vibration response instead of the radiation efficiency, which can be inferred by checking Figure 14b,c. For the radiation efficiency in Figure 14c, when η_R is set to the small value of 0.05, the damping of the resonator only has an observable effect on the radiation efficiency in the frequency

range from 745 to 917 Hz, which is located within or below the band-gap. In this frequency band, the damping of the resonator helps to increase the radiation efficiency, which in turn causes increased radiation over 889–917 Hz. As shown in Figure 15a, with the increase in damping, the radiation efficiency is noticeably increased in the frequency band from 745 to 917 Hz, and is decreased near the frequency of 1130 Hz. However, this decrement is very small, and this will not noticeably affect radiation power.

From the above, it is clear that when damping is not added to the resonator, the attachment of periodic resonators to a sandwich plate helps to reduce sound radiation at frequencies in the band-gap and also close below the band-gap. However, the sound radiation close above the band-gap is significantly enhanced, which leads to poor acoustic performance. This increased acoustic radiation can be further reduced by adding damping to the resonator, which makes the LR sandwich plate more beneficial for noise-reduction purposes.

4. Conclusions

The vibro-acoustic performance of a sandwich plate with periodic resonators was examined in this paper. The band-gap properties, forced response, and acoustic radiation were theoretically derived with closed-form solutions, and were all discussed with the purpose of examining the effects of periodic resonators on the overall acoustic radiation.

For the infinite locally resonant (LR) sandwich plate examined in this paper, a new radiation zone was generated above the band-gap and the coincidence frequency was decreased, resulting in the total effective radiation zone being enlarged. Thus, ineffective radiation in a homogeneous sandwich plate may become effective radiation in an LR sandwich plate. For the finite LR sandwich plate examined in this paper, the periodic resonators had a minimal effect on radiation efficiency in the frequency regions below the fundamental frequency and above the coincidence frequency. Between these two frequencies, the radiation efficiency was decreased below and increased above the resonance frequency of the resonator. The effects of the periodic resonators on radiation efficiency could be physically explained by the effective mass of an LR unit, with decreased mass causing increased radiation efficiency and increased mass causing decreased radiation efficiency. The effective mass can be considered as an indicator of which part of a frequency region will be acoustically improved and which part will be acoustically deteriorated. This will be convenient and important for LR sandwich plate design.

In the band-gap, acoustic radiation is significantly reduced because of the reduction in vibration, as there is no mode existing in the band-gap. In the frequency band close below the band-gap, acoustic radiation is also noticeably reduced, not only because of the suppression of vibration but also because of the lower radiation efficiency. In contrast, the introduction of periodic resonators to a sandwich structure also increases radiation power in the frequency band close above the band-gap, mainly because of the increased radiation efficiency. Fortunately, this increased radiation above the band-gap can be further reduced by introducing a small damping to the resonator by reducing the vibration response. Therefore, in order to improve the acoustic performance of a sandwich plate, the resonator should be tuned at or above the target frequency when damping is not applied in the resonator. When the resonator is damped, the design of band-gap may have more options.

Author Contributions: Conceptualization, Z.G.; data curation, J.P. and M.S.; formal analysis, Z.G.; investigation, J.P.; methodology, Z.G. and M.S.; resources, J.P. and M.S.; software, J.P. and M.S.; supervision, J.P.; validation, Z.G., J.P. and M.S.; visualization, J.P.; writing—original draft, Z.G.; writing—review and editing, J.P. and M.S.

Funding: This research received no external funding.

Acknowledgments: The first author acknowledges both the financial support from the Chinese Scholarship Council and the research-resource support from the University of Western Australia. The authors also gratefully acknowledge the proof reading and language help from Bradley McGrath.

Conflicts of Interest: The authors declare no conflicts of interest.

Appendix A

The elements of operator matrix **L** in Equation (5) are expressed as

$$L_{11} = 2B \frac{\partial^2}{\partial x^2} + 2v_a B \frac{\partial^2}{\partial y^2} - 4G_h + 2\omega^2(m_f + C), \tag{A1}$$

$$L_{12} = 2v_b B \frac{\partial^2}{\partial x \partial y}, \tag{A2}$$

$$L_{13} = 2G_h d \frac{\partial}{\partial x} + 12\omega^2 h_{t1} C \frac{\partial}{\partial x}, \tag{A3}$$

$$L_{21} = L_{12}, \tag{A4}$$

$$L_{22} = 2v_a B \frac{\partial^2}{\partial x^2} + 2B \frac{\partial^2}{\partial y^2} - 4G_h + 2\omega^2(m_f + C), \tag{A5}$$

$$L_{23} = 2G_h d \frac{\partial}{\partial y} + 12\omega^2 h_{t1} C \frac{\partial}{\partial y}, \tag{A6}$$

$$L_{31} = L_{13}, \tag{A7}$$

$$L_{32} = L_{23}, \tag{A8}$$

and

$$L_{33} = 2D \left(\frac{\partial^2}{\partial x^2} + \frac{\partial^2}{\partial y^2} \right)^2 - G_h d^2 \left(\frac{\partial^2}{\partial x^2} + \frac{\partial^2}{\partial y^2} \right) + \omega^2 (2I_f + I_c) \left(\frac{\partial^2}{\partial x^2} + \frac{\partial^2}{\partial y^2} \right) - \omega^2 m_T, \tag{A9}$$

where $v_a = (1 - v_f)/2$, $v_b = (1 + v_f)/2$, $C = m_2/6$, and $h_{t1} = -h_f/12$.

The expressions of K_{ij} and M_{ij} ($i, j = 1, 2, 3$) in Equation (9) are expressed, respectively, as

$$K_{11} = Bk_m^2 + v_a Bk_n^2 + 2G_h, \tag{A10}$$

$$K_{12} = v_b Bk_m k_n, \tag{A11}$$

$$K_{13} = jG_h d k_m, \tag{A12}$$

$$K_{21} = K_{12}, \tag{A13}$$

$$K_{22} = v_a Bk_m^2 + Bk_n^2 + 2G_h, \tag{A14}$$

$$K_{23} = jG_h d k_n, \tag{A15}$$

$$K_{31} = -2jG_h d k_m, \tag{A16}$$

$$K_{32} = -2jG_h d k_n, \tag{A17}$$

$$K_{33} = 2D(k_m^4 + 2k_m^2 k_n^2 + k_n^4) + G_h d^2(k_m^2 + k_n^2), \tag{A18}$$

$$M_{11} = m_f + C, \tag{A19}$$

$$M_{12} = 0, \tag{A20}$$

$$M_{13} = -6j h_{t1} C k_m, \tag{A21}$$

$$M_{21} = 0, \tag{A22}$$

$$M_{22} = m_f + C, \tag{A23}$$

$$M_{23} = -6j h_{t1} C k_n, \tag{A24}$$

$$M_{31} = 12j h_{t1} C k_m, \tag{A25}$$

$$M_{32} = 12jh_{t1}Ck_n, \tag{A26}$$

$$M_{33} = (2I_f + I_c)(k_m^2 + k_n^2) + m_T. \tag{A27}$$

The expressions of a_{ij} in Equation (12) are expressed as

$$a_{11} = B \cos^2 \varphi + v_a B \sin^2 \varphi, \tag{A28}$$

$$a_{12} = 2G_h - \omega^2(m_f + C), \tag{A29}$$

$$a_{13} = v_b B \cos \varphi \sin \varphi, \tag{A30}$$

$$a_{14} = jG_h d \cos \varphi + 6j\omega^2 h_{t1} C \cos \varphi, \tag{A31}$$

$$a_{21} = v_b B \cos \varphi \sin \varphi, \tag{A32}$$

$$a_{22} = v_a B \cos^2 \varphi + B \sin^2 \varphi, \tag{A33}$$

$$a_{23} = 2G_h - \omega^2(m_f + C), \tag{A34}$$

$$a_{24} = jG_h d \sin \varphi + 6j\omega^2 h_{t1} C \sin \varphi, \tag{A35}$$

$$a_{31} = -2jG_h d \cos \varphi + j\omega^2 h_f C \cos \varphi, \tag{A36}$$

$$a_{32} = -2jG_h d \sin \varphi + j\omega^2 h_f C \sin \varphi, \tag{A37}$$

$$a_{33} = 2D, \tag{A38}$$

$$a_{34} = G_h d^2 - \omega^2(2I_f + I_c), \tag{A39}$$

$$a_{35} = \frac{k_R}{ab} - \omega^2 m_T, \tag{A40}$$

$$a_{36} = -\frac{k_R}{ab}, \tag{A41}$$

$$a_{41} = -k_R, \tag{A42}$$

$$a_{42} = k_R - \omega^2 m_R. \tag{A43}$$

The polynomial coefficients in Equation (13) are expressed as $\varepsilon_0 = p_0/p_8$, $\varepsilon_2 = p_2/p_8$, $\varepsilon_4 = p_4/p_8$, and $\varepsilon_6 = p_6/p_8$, where p_0, p_2, p_4, p_6 , and p_8 are expressed, respectively, as

$$p_0 = -a_{12}a_{23}a_{36}a_{41} + a_{12}a_{23}a_{35}a_{42}, \tag{A44}$$

$$p_2 = -a_{12}a_{22}a_{36}a_{41} - a_{11}a_{23}a_{36}a_{41} - a_{14}a_{23}a_{31}a_{42} - a_{12}a_{24}a_{32}a_{42} + a_{12}a_{23}a_{34}a_{42} + a_{12}a_{22}a_{35}a_{42} + a_{11}a_{23}a_{35}a_{42}, \tag{A45}$$

$$p_4 = a_{13}a_{21}a_{36}a_{41} - a_{11}a_{22}a_{36}a_{41} - a_{14}a_{22}a_{31}a_{42} + a_{13}a_{24}a_{31}a_{42} + a_{14}a_{21}a_{32}a_{42} - a_{11}a_{24}a_{32}a_{42} + a_{12}a_{23}a_{33}a_{42} + a_{12}a_{22}a_{34}a_{42} + a_{11}a_{23}a_{34}a_{42} - a_{13}a_{21}a_{35}a_{42} + a_{11}a_{22}a_{35}a_{42}, \tag{A46}$$

$$p_6 = a_{12}a_{22}a_{33}a_{42} + a_{11}a_{23}a_{33}a_{42} - a_{13}a_{21}a_{34}a_{42} + a_{11}a_{22}a_{34}a_{42}, \tag{A47}$$

and

$$p_8 = -a_{13}a_{21}a_{33}a_{42} + a_{11}a_{22}a_{33}a_{42}. \tag{A48}$$

The expressions of \bar{K}_{ij} and \bar{M}_{ij} ($i, j = 1, 2, 3$) in Equation (18) are expressed, respectively, as

$$\bar{K}_{11} = K_{11}, \tag{A49}$$

$$\bar{K}_{12} = K_{12}, \tag{A50}$$

$$\bar{K}_{13} = jK_{13}, \tag{A51}$$

$$\bar{K}_{21} = K_{21}, \quad (\text{A52})$$

$$\bar{K}_{22} = K_{22}, \quad (\text{A53})$$

$$\bar{K}_{23} = jK_{23}, \quad (\text{A54})$$

$$\bar{K}_{31} = -jK_{31}, \quad (\text{A55})$$

$$\bar{K}_{32} = -jK_{32}, \quad (\text{A56})$$

$$\bar{K}_{33} = K_{33}, \quad (\text{A57})$$

$$\bar{M}_{11} = M_{11}, \quad (\text{A58})$$

$$\bar{M}_{12} = M_{12}, \quad (\text{A59})$$

$$\bar{M}_{13} = jM_{13}, \quad (\text{A60})$$

$$\bar{M}_{21} = M_{21}, \quad (\text{A61})$$

$$\bar{M}_{22} = M_{22}, \quad (\text{A62})$$

$$\bar{M}_{23} = jM_{23}, \quad (\text{A63})$$

$$\bar{M}_{31} = -jM_{31}, \quad (\text{A64})$$

$$\bar{M}_{32} = -jM_{32}, \quad (\text{A65})$$

$$\bar{M}_{33} = M_{33}. \quad (\text{A66})$$

References

- Herrmann, A.S.; Zahlen, P.C.; Zuardy, I. Sandwich structures technology in commercial aviation. In Proceedings of the 7th International Conference on Sandwich Structures, Aalborg, Denmark, 29–31 August 2005; pp. 13–26.
- Ning, H.; Janowski, G.M.; Vaidya, U.K.; Husman, G. Thermoplastic sandwich structure design and manufacturing for the body panel of mass transit vehicle. *Compos. Struct.* **2007**, *80*, 82–91. [[CrossRef](#)]
- Mouritz, A.; Gellert, E.; Burchill, P.; Challis, K. Review of advanced composite structures for naval ships and submarines. *Compos. Struct.* **2001**, *53*, 21–42. [[CrossRef](#)]
- Hegger, J.; Horstmann, M. Light-weight TRC sandwich building envelopes. In Proceedings of the Excellence in Concrete Construction through Innovation Conference, London, UK, 9–10 September 2008; pp. 187–194.
- Ferreira, A.; Roque, C.; Jorge, R.; Kansa, E. Static deformations and vibration analysis of composite and sandwich plates using a layerwise theory and multiquadrics discretizations. *Eng. Anal. Bound. Elem.* **2005**, *29*, 1104–1114. [[CrossRef](#)]
- Grover, N.; Maiti, D.; Singh, B. A new inverse hyperbolic shear deformation theory for static and buckling analysis of laminated composite and sandwich plates. *Compos. Struct.* **2013**, *95*, 667–675. [[CrossRef](#)]
- Carrera, E. Historical reviews of zig-zag theories for multilayered plates and shells. *Appl. Mech. Rev.* **2003**, *56*, 287–308. [[CrossRef](#)]
- Hajianmaleki, M.; Qatu, M.S. Vibrations of straight and curved composite beams: A review. *Compos. Struct.* **2013**, *100*, 218–232. [[CrossRef](#)]
- Kirugulige, M.; Kitey, R.; Tippur, H. Dynamic fracture behavior of model sandwich structures with functionally graded core: A feasibility study. *Compos. Sci. Technol.* **2005**, *65*, 1052–1068. [[CrossRef](#)]
- Kazancı, Z.; Mecitoğlu, Z. Nonlinear dynamic behavior of simply supported laminated composite plates subjected to blast load. *J. Sound Vib.* **2008**, *317*, 883–897. [[CrossRef](#)]
- Park, T.; Lee, S.; Seo, J.; Voyiadjis, G. Structural dynamic behavior of skew sandwich plates with laminated composite faces. *Compos. Part B Eng.* **2008**, *39*, 316–326. [[CrossRef](#)]
- Allahverdizadeh, A.; Mahjoob, M.; Maleki, M.; Nasrollahzadeh, N.; Naei, M. Structural modeling, vibration analysis and optimal viscoelastic layer characterization of adaptive sandwich beams with electrorheological fluid core. *Mech. Res. Commun.* **2013**, *51*, 15–22. [[CrossRef](#)]

13. Piana, E.A.; Petrogalli, C.; Paderno, D.; Carlsson, U. Application of the wave propagation approach to sandwich structures: Vibro-acoustic properties of aluminum honeycomb materials. *Appl. Sci.* **2018**, *8*, 45. [[CrossRef](#)]
14. Adessina, A.; Hamdaoui, M.; Xu, C. Damping properties of bi-dimensional sandwich structures with multi-layered frequency-dependent visco-elastic cores. *Compos. Struct.* **2016**, *154*, 334–343. [[CrossRef](#)]
15. Chen, D.; Kitipornchai, S.; Yang, J. Nonlinear free vibration of shear deformable sandwich beam with a functionally graded porous core. *Thin Wall Struct.* **2016**, *107*, 39–48. [[CrossRef](#)]
16. Chikh, N.; Nour, A.; Aguib, S.; Tawfiq, I. Dynamic analysis of the non-linear behavior of a composite sandwich beam with a magnetorheological elastomer core. *Acta Mech. Solida Sin.* **2016**, *29*, 271–283. [[CrossRef](#)]
17. Fortini, M.; Granzotto, N.; Piana, E.A. Vibro-acoustic characterization of a composite structure featuring an innovative phenolic foam core. *Appl. Sci.* **2019**, *9*, 1276. [[CrossRef](#)]
18. Sikdar, S.; Banerjee, S. Guided wave propagation in a honeycomb composite sandwich structure in presence of a high density core. *Ultrasonics* **2016**, *71*, 86–97. [[CrossRef](#)] [[PubMed](#)]
19. Bapanapalli, S.K.; Martinez, O.M.; Gogu, C.; Sankar, B.V.; Haftka, R.T.; Blosser, M.L. Analysis and design of corrugated core sandwich panels for thermal protection systems of space vehicles. In Proceedings of the 47th AIAA/ASME/ASCE/AHS/ASC Structures, Structural Dynamics, and Materials Conference, Newport, Rhode Island, 1–4 May 2006; pp. 1–18.
20. Munch-Andersen, J. Improving thermal insulation of concrete sandwich buildings. *Indoor Built Environ.* **2009**, *18*, 424–431. [[CrossRef](#)]
21. Denli, H.; Sun, J. Structural-acoustic optimization of sandwich structures with cellular cores for minimum sound radiation. *J. Sound Vib.* **2007**, *301*, 93–105. [[CrossRef](#)]
22. Franco, F.; Cunefare, K.A.; Ruzzene, M. Structural-acoustic optimization of sandwich panels. *J. Vib. Acoust.* **2007**, *129*, 330–340. [[CrossRef](#)]
23. Wang, T.; Li, S.; Nutt, S.R. Optimal design of acoustical sandwich panels with a genetic algorithm. *Appl. Acoust.* **2009**, *70*, 416–425. [[CrossRef](#)]
24. Ni, Q.; Xiang, Y.; Huang, Y.; Lu, J. Modeling and dynamics analysis of shells of revolution by partially active constrained layer damping treatment. *Acta Mech. Solida Sin.* **2013**, *26*, 468–479. [[CrossRef](#)]
25. Datta, P.; Ray, M. Three-dimensional fractional derivative model of smart constrained layer damping treatment for composite plates. *Compos. Struct.* **2015**, *156*, 291–306. [[CrossRef](#)]
26. Narayanamurti, V.; Störmer, H.; Chin, M.; Gossard, A.; Wiegmann, W. Selective transmission of high-frequency phonons by a superlattice: The “dielectric” phonon filter. *Phys. Rev. Lett.* **1979**, *43*, 2012–2016. [[CrossRef](#)]
27. Liu, Z.; Zhang, X.; Mao, Y.; Zhu, Y.; Yang, Z.; Chan, C.; Sheng, P. Locally resonant sonic materials. *Science* **2000**, *289*, 1734–1736. [[CrossRef](#)] [[PubMed](#)]
28. Hussein, M.I.; Leamy, M.J.; Ruzzene, M. Dynamics of phononic materials and structures: Historical origins, recent progress, and future outlook. *Appl. Mech. Rev.* **2014**, *66*, 040802. [[CrossRef](#)]
29. Smith, D.R.; Pendry, J.B.; Wiltshire, M.C. Metamaterials and negative refractive index. *Science* **2004**, *305*, 788–792. [[CrossRef](#)] [[PubMed](#)]
30. Del Vescovo, D.; Giorgio, I. Dynamic problems for metamaterials: Review of existing models and ideas for further research. *Int. J. Eng. Sci.* **2014**, *80*, 153–172. [[CrossRef](#)]
31. Deymier, P.A. *Acoustic Metamaterials and Phononic Crystals*; Springer Science & Business Media: New York, NY, USA, 2013.
32. Kushwaha, M.S.; Halevi, P.; Dobrzynski, L.; Djafari-Rouhani, B. Acoustic band structure of periodic elastic composites. *Phys. Rev. Lett.* **1993**, *71*, 2022–2025. [[CrossRef](#)] [[PubMed](#)]
33. Wu, J.; Bai, X.; Xiao, Y.; Geng, M.; Yu, D.; Wen, J. Low frequency band gaps and vibration reduction properties of a multi-frequency locally resonant phononic plate. *Acta Phys. Sin.* **2015**, *65*, 064602.
34. Yu, D.; Liu, Y.; Qiu, J.; Zhao, H.; Liu, Z. Experimental and theoretical research on the vibrational gaps in two-dimensional three-component composite thin plates. *Chin. Phys. Lett.* **2005**, *22*, 1958–1960.
35. Zhao, H.; Wen, J.; Yu, D.; Wen, X. Low-frequency acoustic absorption of localized resonances: Experiment and theory. *J. Appl. Phys.* **2010**, *107*, 023519. [[CrossRef](#)]
36. Meng, H.; Wen, J.; Zhao, H.; Wen, X. Optimization of locally resonant acoustic metamaterials on underwater sound absorption characteristics. *J. Sound Vib.* **2012**, *331*, 4406–4416. [[CrossRef](#)]
37. Zhang, S.; Wu, J.H.; Hu, Z. Low-frequency locally resonant band-gaps in phononic crystal plates with periodic spiral resonators. *J. Appl. Phys.* **2013**, *113*, 163511. [[CrossRef](#)]

38. Nouh, M.; Aldraihem, O.; Baz, A. Wave propagation in metamaterial plates with periodic local resonances. *J. Sound Vib.* **2015**, *341*, 53–73. [[CrossRef](#)]
39. Hsu, J.C. Local resonances-induced low-frequency band gaps in two-dimensional phononic crystal slabs with periodic stepped resonators. *J. Phys. D Appl. Phys.* **2011**, *44*, 055401. [[CrossRef](#)]
40. Xiao, Y.; Wen, J.; Wen, X. Sound transmission loss of metamaterial-based thin plates with multiple subwavelength arrays of attached resonators. *J. Sound Vib.* **2012**, *331*, 5408–5423. [[CrossRef](#)]
41. Xiao, Y.; Wen, J.; Yu, D.; Wen, X. Flexural wave propagation in beams with periodically attached vibration absorbers: Band-gap behavior and band formation mechanisms. *J. Sound Vib.* **2013**, *332*, 867–893. [[CrossRef](#)]
42. Wang, Y.F.; Wang, Y.S. Complete bandgaps in two-dimensional phononic crystal slabs with resonators. *J. Appl. Phys.* **2013**, *114*, 043509. [[CrossRef](#)]
43. Chen, J.; Sun, C. Dynamic behavior of a sandwich beam with internal resonators. *J. Sandw. Struct. Mater.* **2011**, *13*, 391–408. [[CrossRef](#)]
44. Chen, J.; Sharma, B.; Sun, C. Dynamic behaviour of sandwich structure containing spring-mass resonators. *Compos. Struct.* **2011**, *93*, 2120–2125. [[CrossRef](#)]
45. Chen, J.; Sun, C. Wave propagation in sandwich structures with resonators and periodic cores. *J. Sandw. Struct. Mater.* **2013**, *15*, 359–374. [[CrossRef](#)]
46. Chen, J.; Wang, R. Wave propagation and power flow analysis of sandwich structures with internal absorbers. *J. Vib. Acoust.* **2014**, *136*, 041003. [[CrossRef](#)]
47. Chen, J.; Huang, Y. Wave propagation in sandwich structures with multiresonators. *J. Vib. Acoust.* **2016**, *138*, 041009. [[CrossRef](#)]
48. Chen, J.; Tsai, S. Sandwich structures with periodic assemblies on elastic foundation under moving loads. *J. Vib. Control* **2016**, *22*, 2519–2529. [[CrossRef](#)]
49. Sharma, B.; Sun, C. Local resonance and Bragg bandgaps in sandwich beams containing periodically inserted resonators. *J. Sound Vib.* **2016**, *364*, 133–146. [[CrossRef](#)]
50. Xie, G.; Thompson, D.; Jones, C. The radiation efficiency of baffled plates and strips. *J. Sound Vib.* **2005**, *280*, 181–209. [[CrossRef](#)]



© 2019 by the authors. Licensee MDPI, Basel, Switzerland. This article is an open access article distributed under the terms and conditions of the Creative Commons Attribution (CC BY) license (<http://creativecommons.org/licenses/by/4.0/>).